

Transient Interporosity Flow in Shale/Tight Oil Reservoirs: Model and Application

Shan Huang,* Xinhua Ma, Rui Yong, Jianfa Wu, Jian Zhang, and Tianpeng Wu

Cite This: *ACS Omega* 2022, 7, 14746–14755

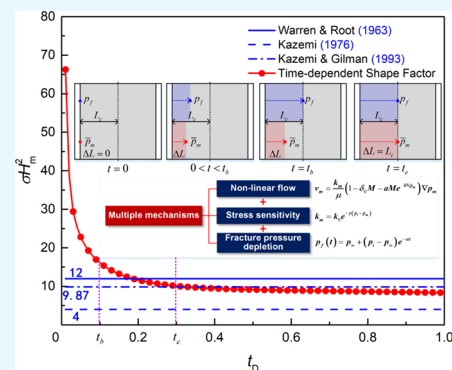
Read Online

ACCESS |

Metrics & More

Article Recommendations

ABSTRACT: The dual-porosity model has been used widely to describe the fracture network in well test or numerical simulation due to the high computational efficiency. The shape factor, which can be used to determine the capability of mass transfer between the matrix and fracture, is the core of the dual-porosity model. However, the conventional shape factor, which is usually obtained under pseudo-steady state assumption, has certain limitation in characterization of the mass transfer efficiency in a shale/tight reservoir. In this study, a new transient interporosity flow model has been established by considering the influence of nonlinear flow, stress sensitivity, and fracture pressure depletion. To solve this new model, a finite difference and Newton iteration method was applied. According to the Duhamel principle, the solution for time-dependent fracture pressure boundary condition has been obtained. The solution has been verified by using the fine-grid finite element method. Then, the influence of nonlinear flow, stress sensitivity, and fracture pressure depletion on shape factor and interporosity flow rate has been studied. The study results show that constant shape factors are not suitable for unconventional reservoirs, and the interporosity flow in the shale/tight reservoir is controlled by multiple factors. The new model can be used in test interpretation and numerical simulation, and also provides a new approach for the optimization of the perforation cluster number.



1. INTRODUCTION

Shale/tight reservoirs are characterized by low permeability and low porosity,¹ and multicluster fracturing with a horizontal well is effective for the development of such reservoirs.^{2,3} Stimulated reservoir volume (SRV) is formed after fracturing. There are

many methods to characterize the SRV zone, such as the unstructured perpendicular bisection (PEBI) grid, discrete fracture networks (DFN), and embedded-discrete-fracture model (EDFM).⁴ However, in well test models or numerical simulation models, the dual-porosity model is still widely used to compromise between accuracy and computational efficiency. To overcome the high in situ stress and horizontal stress difference and to improve the complexity of the fracture, multicluster fracture with tight cutting has been used in recent years.⁵ The flow between the perforation tunnel and matrix can also be characterized by the dual-porosity model, which can provide the possibility to optimize the number of perforation clusters.

The concept of the dual-porosity model was first proposed by Barenblatt et al.⁶ They divided the fractured reservoirs into two flow systems, namely, the matrix system and the natural fracture system. The following transfer function connects these two flow systems:

Table 1. Constant Shape Factor by Various Researchers

investigator(s)	time	method	dimensions		
			1D	2D	3D
Warren and Root ⁷	1963	geometrical	12	32	60
Kazemi et al. ⁸	1976	numerical	4	8	12
Thomas et al. ⁹	1983	numerical			25
Ueda et al. ¹⁰	1989	numerical	8	24	
Coats ¹¹	1989	numerical	8	16	24
de Swaan ¹²	1990	analytical	15		60
Kazemi and Gilman ¹³	1993	analytical	9.87	19.74	29.61
Zimmerman et al. ¹⁴	1993	analytical	9.87	18.17	29.61
Lim and Aziz ²¹	1995	analytical	9.87	18.17	25.67
Quintard and Whitaker ¹⁵	1996	averaging	12	28.45	49.58
Bourbiaux et al. ¹⁶	1999	numerical		20	
Noetinger et al. ¹⁷	2000	random walk	11.5	27.1	
Sarda et al. ¹⁸	2002	numerical	8	24	48
Rasmussen and Civan ¹⁹	2003	analytical	9.87	18.17	25.67

Received: January 3, 2022

Accepted: April 7, 2022

Published: April 19, 2022



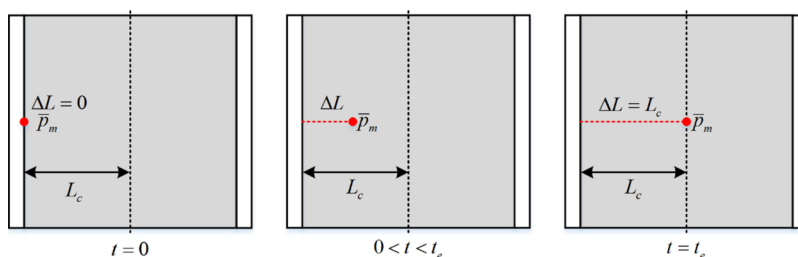


Figure 1. Schematic diagram of the average matrix pressure.

$$q = \frac{\sigma k_m V}{\mu} (\bar{p}_m - p_f) \quad (1)$$

where q is the interporosity rate, $10^{-6} \text{ m}^3/\text{s}$; σ is the shape factor, m^{-2} ; V is the volume of the matrix block, m^3 ; k_m is the matrix permeability, $10^{-3} \mu\text{m}^2$; μ is the fluid viscosity, $\text{mPa}\cdot\text{s}$; \bar{p}_m is the volumetric average matrix pressure, MPa ; p_f is the fracture pressure, MPa .

During early research, the shape factor was commonly obtained based on the pseudo-steady state assumption, leading to a constant shape factor. The shape factors obtained by different researchers are summarized in Table 1.^{7–19,21} However, the constant shape factor has some defects in characterization of the transient flow features.

To overcome the shortcomings of the pseudo-steady state method, an unsteady-state diffusion equation was then used by several researchers, leading to a time-dependent shape factor. The research on the time-dependent shape factor was first started by Chang.²⁰ By solving the three-dimensional pressure diffusion equations under unsteady-state conditions, a series of shape factors at constant fracture pressure or constant flow rate were obtained. He proposed that the value of the shape factor decreased and tended to be constant when the flow state gradually reached the pseudo-steady state. The stabilized values of the shape factors were the same as the values obtained by Kazemi and Gilman. To obtain an approximate analytical solution, Lim and Aziz²¹ used an exponential function to solve the pressure diffusion equation without using the pseudo-steady state assumption. By extracting the first term of the infinite summation series, they obtained the constant shape factors. Rangel-German and Kovscek²² proposed a piecewise function for cubic matrix blocks based on the imbibition experiment. A power function was used to characterize the unsteady state. Hassanzadeh and Pooladi-Darvish²³ solved pressure diffusion equations under different fracture boundary conditions and coordinate systems by using Laplace transform and Duhamel's principle. Their study results reveal that the value of the shape factor is influenced by the pressure depletion regime of fractures. Based on their work, Ranjbar et al.^{24,25} obtained the shape factor of compressible fluid under different pressure depletion regimes for one-dimensional conditions. He et al.^{26,27} further obtained the constant and time-dependent shape factors by considering the influence of tortuosity and threshold pressure based on Lim and Aziz's work. By considering the stress sensitivity of the tight reservoir, Wang et al.^{28,29} established an unsteady interporosity model and obtained the time-dependent shape factor. Liu et al.³⁰ designed some experiments to investigate the influence of stress sensitivity on interporosity flow. Rostami et al.³¹ have calculated the shape factors for multidimensional irregular bodies in a systematic approach by using fine-grid simulation. Abbasi et al.³² obtained the time-dependent shape factor by considering the influence of the quadrature pressure gradient, the heterogeneous

matrix, and the pressure-dependent rock properties. In addition, scholars have studied the influence of condensation,³³ capillary imbibition process,³⁴ gravity drainage,³⁵ and nonisothermal process³⁶ on the interporosity flow, and the corresponding time-dependent shape factors have been obtained.

Although scholars mentioned above have carried out a detailed studies about the shape factor, the existing shape factors ignored the unique seepage mechanisms of shale/tight oil reservoirs, such as nonlinear flow and stress sensitivity. Additionally, the fracture pressure was mostly considered as a constant in previous studies. To overcome these shortcomings, a new transient interporosity flow model has been established by considering the influence of nonlinear flow, stress sensitivity, and time-dependent fracture pressure boundary conditions. The model was solved by using finite difference and Newton iteration method. By using the Duhamel principle, the solution of time-dependent fracture pressure boundary condition was obtained. Then, sensitivity analysis of the shape factor and the interporosity flow rate was conducted. Finally, the new model was used in well test interpretation and perforation cluster number optimization.

2. METHODOLOGY

The transfer function can also be expressed as a form of Darcy's law:

$$q = \frac{k_m A}{\mu} \frac{(\bar{p}_m - p_f)}{\Delta L} \quad (2)$$

where A is the cross-sectional area of the matrix block, m^2 ; ΔL is the characteristic length which is defined as the distance between p_f and \bar{p}_m , m .

We get the following equation by combining eqs 1 and 2:

$$\sigma = \frac{A}{V \Delta L} \quad (3)$$

As shown in eq 3, the shape factor is the ratio of the cross-sectional area for fluid transfer to the characteristic flow distance under unit volume, and it is a parameter related to several geometric factors. A/V can be used to reflect the geometric features of the matrix block. $1/\Delta L$ can be used to control the fluid exchange between the matrix and fracture.

As seen in Figure 1, at the initial moment, the pressure in the matrix is the initial reservoir pressure. The location of the average matrix pressure \bar{p}_m is at the fracture surface, and $\Delta L = 0$. With the decreasing of \bar{p}_m , the location of \bar{p}_m moves toward the center of the matrix block, and the value of ΔL increases, which leads to a decrease of the shape factor σ . It can be seen from the symmetry that there is no fluid flow in the center of the matrix. The pseudo-steady state is reached when the location of \bar{p}_m reaches the center of the matrix block. At this time (t_e), ΔL is equal to L_c and the value of σ becomes constant.

The fluid volume of interporosity flow from the matrix to fracture is equal to the expanded volume of the fluid in the matrix due to the pressure drop, according to the law of conservation of mass. Hence, the interporosity flow rate can be expressed as:

$$q = -V\phi_m c_t \frac{\partial \bar{p}_m}{\partial t} \quad (4)$$

Combining eqs 1 and 4, we get the following equation:

$$\sigma = -\frac{1}{\eta(\bar{p}_m - p_f)} \frac{\partial \bar{p}_m}{\partial t} \quad (5)$$

where $\eta = k_m/(\phi_m \mu c_t)$ is the hydraulic diffusivity, m^2/s .

Equation 5 can be used to calculate the value of the time-dependent shape factor when the relationship between average matrix pressure and time is obtained.

Nonlinear flow in a shale/tight reservoir is caused by the boundary layer.³⁷ To characterize the nonlinear flow in shale/tight formation, Huang et al.^{38,39} established a new seepage model based on the capillary bundle model and the fractal theory. The thickness of the boundary layer δ can be described by exponential function $\delta = \delta_0 + ae^{-b \nabla p}$. According to Huang's study, the motion equation in the matrix is:

$$v_m = \frac{k_m}{\mu} (1 - \delta_0 M - a M e^{-b \nabla p_m}) \nabla p_m \quad (6)$$

where v_m is the fluid's velocity in the matrix, m/s ; μ is the viscosity, $mPa \cdot s$; k_m is the matrix permeability, mD ; ∇p_m is the pressure gradient in the matrix, MPa/m ; $M = 4(3 - D_f + D_T)/[r_{max}(2 - D_f + D_T)]$ is the nonlinear coefficient; δ_0 is the thickness of stable layer; a and b are the boundary layer coefficients; D_f is the pore fractal dimension; D_T is the tortuosity fractal dimension; r_{max} is the maximum pore radius of the reservoir, μm . δ_0 , a , and b can be obtained by the nonlinear flow experiment. r_{max} , D_f and D_T can be obtained by mercury intrusion porosimetry.

To account for the influence of effective stress on matrix permeability, a stress-dependent permeability is used. According to previous research studies,⁴⁰ there is an exponential relationship between permeability and pressure, which is given as:

$$k_m = k_0 e^{-\gamma(p_i - p_m)} \quad (7)$$

where k_0 is the initial permeability of the matrix, $10^{-3} \mu m^2$; γ is the permeability modulus, MPa^{-1} ; p_i is the initial pressure of the reservoir, MPa ; p_m is the matrix pressure, MPa .

During the development of shale/tight reservoirs, the fracture pressure is not constant and decreases over time. The research conducted by Ranjbar et al. shows that the exponential decline of fracture pressure is more in line with the field conditions. We assumed that the initial fracture pressure equals the initial pressure p_i and decreases exponentially with time:

$$p_f(t) = p_\infty + (p_i - p_\infty) e^{-\alpha t} \quad (8)$$

where $p_\infty = p_f|_{t \rightarrow \infty}$; α is the decline constant, s^{-1} .

3. MATHEMATICAL MODEL

The matrix–fracture system is shown in Figure 2. On both sides of the matrix, there are two parallel fractures. The matrix pressure satisfies the following equation:

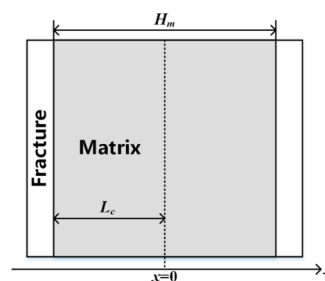


Figure 2. Illustration of a matrix–fracture system.

Table 2. Definition of Dimensionless Variables

name	expression
dimensionless pressure	$p_D = \frac{p - p_i}{p_\infty - p_i}$
dimensionless time	$t_D = \frac{\eta_0 t}{L_c^2}$
dimensionless distance	$x_D = \frac{x}{L_c}$
dimensionless permeability modulus	$\gamma_{mD} = \gamma(p_i - p_\infty)$
dimensionless decline constant	$\kappa = \frac{L_c^2}{\eta_0} \alpha$
dimensionless interporosity flow rate	$q_D = -\frac{\mu L_c^2}{k_0 V (p_\infty - p_i)} q$

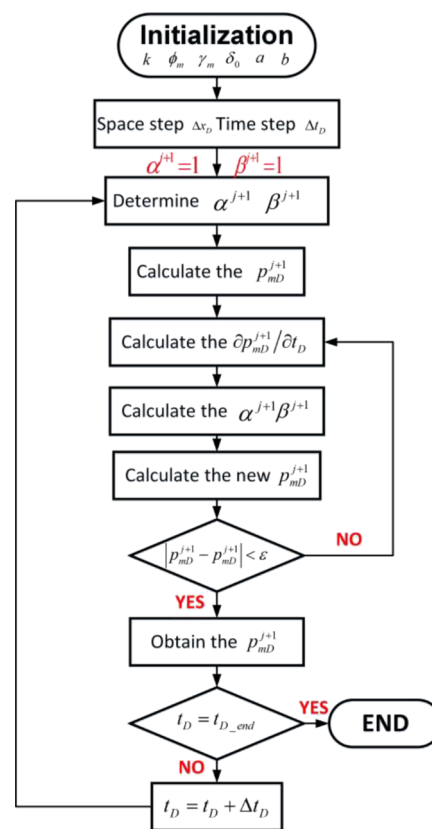


Figure 3. Computational procedure of the model.

$$\frac{\partial}{\partial x} \left[\frac{k_0 e^{-\gamma(p_i - p_m)} (1 - \delta_0 M - a M e^{-b \partial p_m / \partial x})}{\phi_m \mu c_t} \frac{\partial p_m}{\partial x} \right] = \frac{\partial p_m}{\partial t} \quad (9)$$

where c_t is the total compressibility, MPa^{-1} ; ϕ_m is the porosity of the matrix.

The abovementioned function can be simplified as:

$$\bar{p}_{mD_Depletion}(t_D) = \int_0^1 p_{mD_Depletion} dx_D \quad (22)$$

The dimensionless shape factor σH_m^2 and the dimensionless interporosity flow rate q_D can be obtained by nondimensionalizing eqs 4 and 5:

$$\sigma H_m^2 = -\frac{4}{(\bar{p}_{mD} - p_{fD})} \frac{\partial \bar{p}_{mD}}{\partial t_D} \quad (23)$$

$$q_D = \frac{\partial \bar{p}_{mD}}{\partial t_D} \quad (24)$$

Finally, σH_m^2 and q_D can be obtained by substituting $\bar{p}_{mD_Depletion}(t_D)$ to eqs 23 and 24.

4. VALIDATION

To validate this model, a numerical model has been established by using the fine-grid finite element method (FEM), as shown in

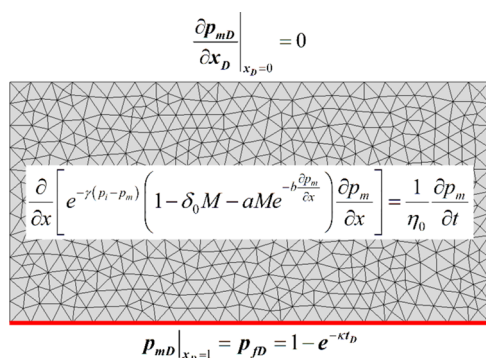


Figure 4. Schematic of the numerical model developed by the fine-grid element method.

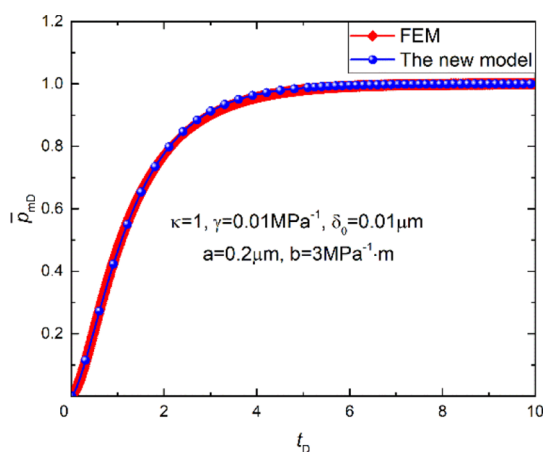


Figure 5. Comparison of the average matrix pressure calculated by the new model and the result obtained from the FEM.

Figure 4. The parameters used for comparison are: $L_c = 10$ m, $p_i = 20$ MPa, $p_\infty = 10$ MPa, $k_0 = 0.1$ mD, $\phi_m = 0.1$, $\mu = 1$ mPa·s, $c_t = 4 \times 10^{-4}$ MPa $^{-1}$, $\delta_0 = 0.01$ μ m, $a = 0.2$ μ m, $b = 3$ MPa $^{-1}$ ·m, $\gamma_m = 0.01$ MPa $^{-1}$, and $\kappa = 1$. Then we compared the average matrix pressure calculated by this model with the results obtained by the fine-grid finite element simulation. As illustrated in **Figure 5**, the new model's solution is consistent with the results of the finite element simulation. In addition, a relatively simple case

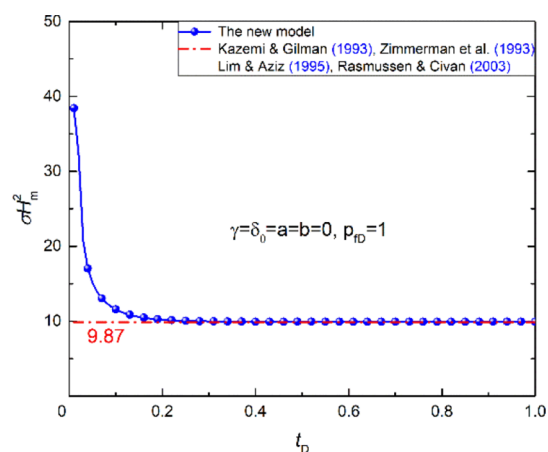


Figure 6. Comparison of the time-dependent shape factor calculated by the new model and the result obtained by researchers.^{13,14,19,21}

without considering any mechanism was conducted and a comparison was made with previous research studies. The stabilized value of the time-dependent shape factor calculated by the new model is in good accordance with the shape factor obtained by researchers such as Kazemi and Gilman and Lim and Aziz (**Figure 6**). Therefore, the solution in this study is accurate and reliable.

5. RESULTS AND DISCUSSION

5.1. Sensitivity Analysis. To better understand the influence of nonlinear flow, stress sensitivity, and fracture

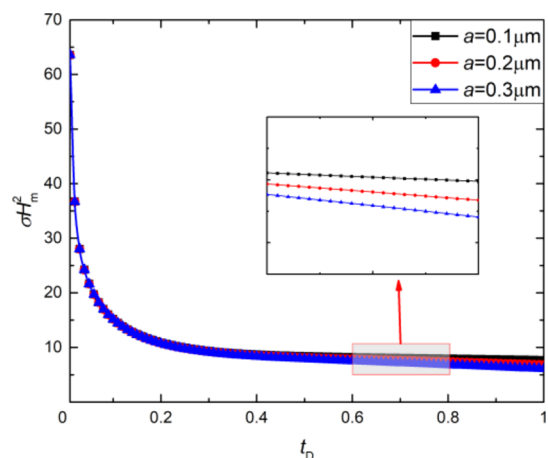


Figure 7. Comparison of the dimensionless shape factor for different a .

pressure depletion on the dimensionless shape factor (σH_m^2), five factors have been selected for sensitivity analysis, which are γ_m , δ_0 , a , b , and κ .

As shown in **Figure 7**, the larger the boundary layer coefficient a is, the smaller the dimensionless shape factor is. The influence of coefficient a is not obvious at first, but increases with time. This is due to the fact that the pressure gradient in the matrix is the largest at the beginning, which weakens the influence of the coefficient a to the greatest extent. As the interporosity flow proceeds, the average matrix pressure \bar{p}_m and the pressure gradient $d\bar{p}_m/dx$ decreases, resulting in a more significant influence of the coefficient a .

It can be seen from **Figure 8** that the dimensionless shape factor increases with the increase of coefficient b . b is the

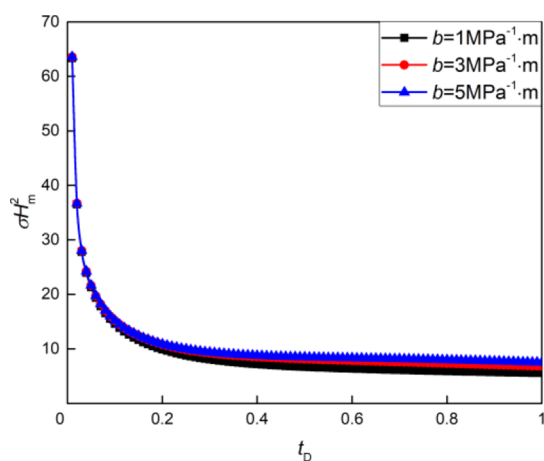


Figure 8. Comparison of the dimensionless shape factor for different b .

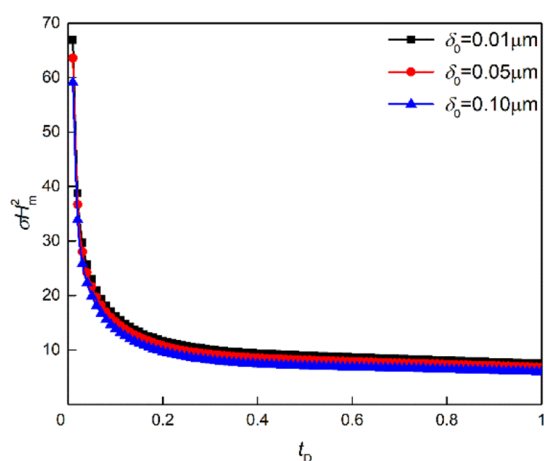


Figure 9. Comparison of the dimensionless shape factor for different δ_0 .

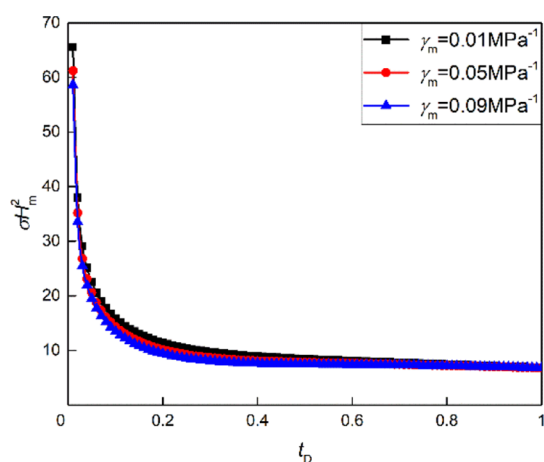


Figure 10. Comparison of the dimensionless shape factor for different γ_m .

coefficient directly acting on the pressure gradient. The larger the value of coefficient b is, the greater the influence of the pressure gradient on the thickness of the boundary layer and the weaker the influence of nonlinear flow.

The influence of the thickness of stable layer δ_0 is the most significant and continuous through the entire flow stage, as shown in Figure 9. The larger the δ_0 is, the smaller the dimensionless shape factor is.

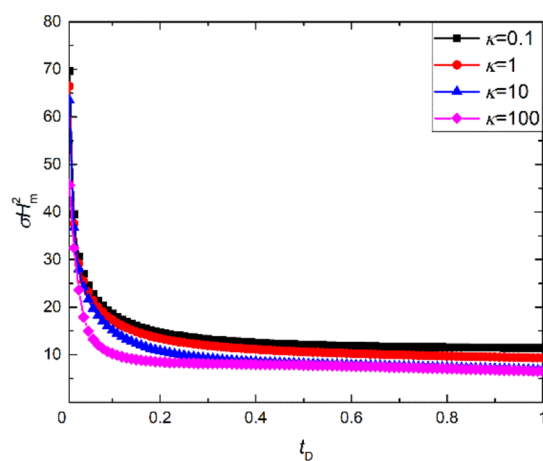


Figure 11. Comparison of the dimensionless shape factor for different κ .

Table 3. Experimental Design

level	factors				
	δ_0 (μm)	a (μm)	b ($\text{MPa}^{-1}\cdot\text{m}$)	γ_m (MPa^{-1})	κ
1	0.01	0.1	2	0.01	1
2	0.01	0.1	2	0.03	10
3	0.01	0.2	4	0.01	1
4	0.01	0.2	4	0.03	10
5	0.03	0.1	4	0.01	10
6	0.03	0.1	4	0.03	1
7	0.03	0.2	2	0.01	10
8	0.03	0.2	2	0.03	1

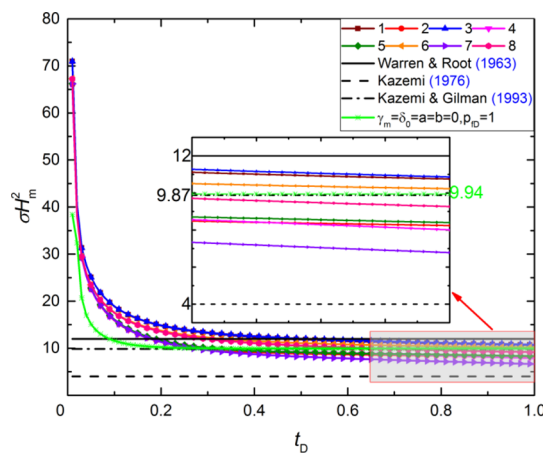


Figure 12. Comparison of the dimensionless shape factor under different conditions.

Figure 10 indicates that the stress sensitivity affects the early stage ($t_D \leq 0.2$) of the interporosity flow, which is different from the influence of nonlinear flow. This is consistent with the variation of matrix permeability with stress.

The dimensionless shape factor calculated under different dimensionless decline constant κ is shown in Figure 11. The larger the decline coefficient, the faster the decline speed of the fracture pressure and the smaller the value of σH_m^2 . What is more, with increasing of κ , the decline speed of σH_m^2 becomes faster and the transient stage becomes shorter.

5.2. Control Mechanisms of Multiple Factors. To further evaluate the comprehensive influence of nonlinear flow, stress

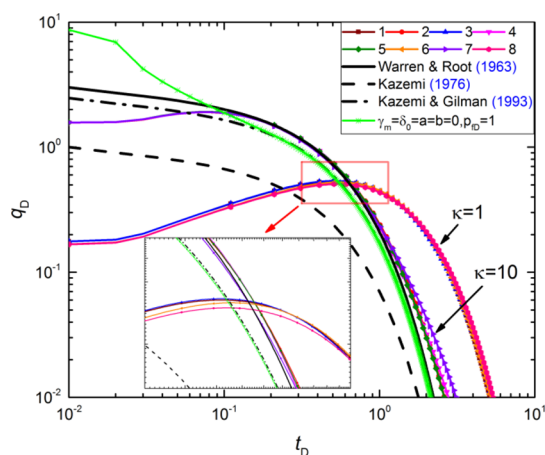


Figure 13. Comparison of the dimensionless interporosity flow rate under different conditions.

sensitivity, and fracture pressure depletion on the dimensionless shape factor (σH_m^2) and the dimensionless interporosity flow rate (q_D), two different levels are taken for each factor. The following eight schemes have been designed according to the orthogonal table $L_8(4^1 \times 2^4)$, which is shown in Table 3.

The dimensionless shape factors of Schemes 1–8 are shown in Figure 12. Due to the least influence of nonlinear flow and stress sensitivity, and the slowest rate of fracture pressure depletion, Scheme 3 has the highest shape factor. On the contrary, Scheme 7 has the smallest shape factor. The value of the shape factor is found to be less when the influence of nonlinear flow and stress sensitivity is higher. The value of the shape factor is larger because the fracture pressure depletion rate is smaller. In addition, the unsteady stage becomes longer after considering the influence of nonlinear flow, stress sensitivity, and fracture pressure depletion. Constant shape factors (refs 7, 8, 13) will greatly underestimate the rate of the interporosity flow at the initial stage. The stabilized value of Schemes 1–8 is between Kazemi and Warren and Root's constant shape factors. The shape factor of Warren and Root will be larger at the later stage. The shape factor of Kazemi is only 1/3 of the shape factor of Warren and Root, which is always small. The shape factor of Kazemi and Gilman is basically the same as the shape factor when $\gamma_m = \delta_0 = a = b = 0$ and $p_{FD} = 1$. The greater the influence of nonlinear flow and stress sensitivity, the greater the deviation from Kazemi and Gilman's shape factor.

The dimensionless interporosity flow rate of Schemes 1–8 is shown in Figure 13. The smaller the influence of nonlinear flow and stress sensitivity is, the higher the interporosity flow rate is at the initial stage. However, the interporosity flow rate decreases faster. When the decline constant is larger, the interporosity flow rate is larger at the early stage but smaller at the later stage. The initial interporosity flow rate will be significantly smaller after considering the influence of nonlinear flow, stress sensitivity, and fracture pressure depletion. It has been found that the constant shape factor will greatly underestimate the interporosity flow rate between matrix and fractures at the initial stage compared with the conventional time-dependent shape factor ($\gamma_m = \delta_0 = a = b = 0$ and $p_{FD} = 1$). However, the value of the interporosity flow rate at the initial stage may be less than that calculated by the constant shape factor after considering the influence of multiple factors. Therefore, mass transfer between the matrix and fractures is controlled by multiple mechanisms for shale/tight reservoirs. Neither constant shape factor nor conventional time-dependent shape factor can be used to characterize accurately the mass transfer efficiency between the matrix and fracture in a shale/tight reservoir.

6. APPLICATION

6.1. Well Test Interpretation. We have established a trilinear flow model in previous research studies.^{42,43} Figure 14 is

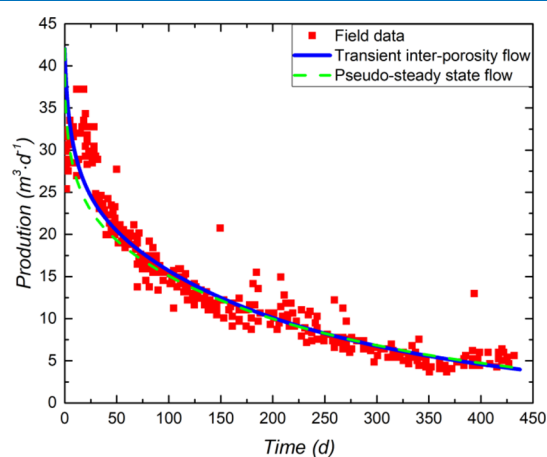


Figure 15. Matching result of production from Well CARD-1.

the schematic diagram of the trilinear flow model. It is assumed that all fractures are equally spaced along the horizontal well,

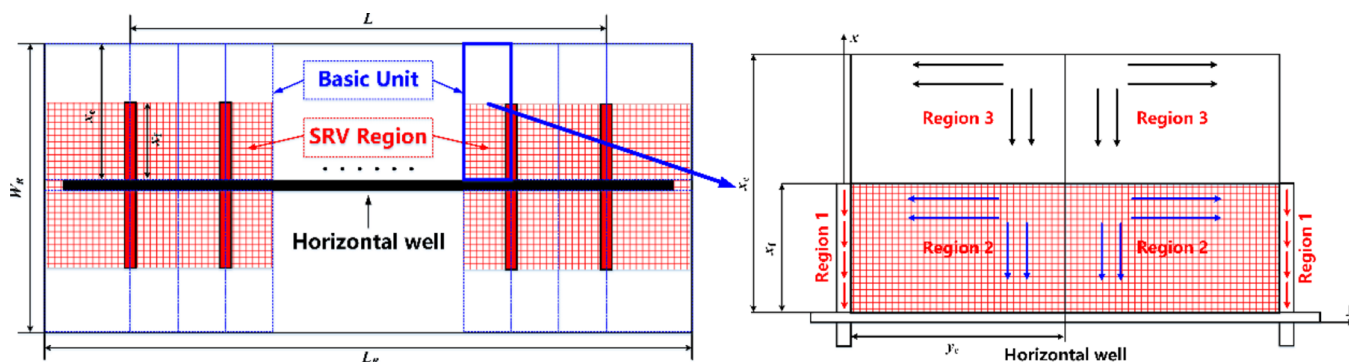


Figure 14. Schematic diagram of the trilinear flow model for a multifractured horizontal well.⁴² Reprinted with permission from ref 42. Copyright of 2018/Saudi Society for Geosciences, Springer Nature/ Saudi Society for Geosciences.

relevant parameters are listed in Table 6. The cumulative production of each matrix was obtained by integrating the interporosity rate. Then, the cumulative production of the unit with different perforation cluster numbers was obtained. The time for pressure diffusion to the no-flow boundary was obtained by analyzing the pressure feature of the grid where the nonflow boundary is located. Finally, the type curve for optimization of the perforation cluster number was drawn, as shown in Figure 17.

The cumulative production increased with the increasing in the perforation cluster number, but the growth rate slowed down gradually. The shorter the production time, the greater the difference in cumulative production under different perforation cluster numbers. However, the difference gradually decreased with the increase in the production time. In addition, the time for matrix pressure diffusion to the no-flow boundary between perforation clusters (t_{ei}) was different from the time for that outside perforation clusters (t_{eo}). When the number of perforation clusters is small, the difference between t_{ei} and t_{eo} is great, leading to an unbalanced utilization of the fracturing unit. On the contrary, there will be mutual interference between perforation clusters in a very short time when the number of perforation clusters is large. Therefore, there is an optimal value for the perforation cluster number. For example, in Figure 17, the optimal perforation cluster number is 4 or 5, which can balance production and interference. It is important to note that this only provides a new idea for optimization of the perforation cluster number. It is necessary to consider comprehensively the influence of multiple factors during the optimization process, such as in situ stress and fracturing parameters.

7. CONCLUSIONS

In this study, a transient interporosity flow model has been established. In this model, the nonlinear flow and stress sensitivity of the shale/tight oil reservoirs have been taken into account. Moreover, the influence of fracture pressure depletion has also been taken into account. Finite difference, Newton iteration method, and Duhamel principle have been used to solve the new model. The study results show that the fluid flow between matrix and fracture in a shale/tight reservoir is controlled by multiple factors. The interporosity flow rate at the initial stage might be underestimated when constant shape factors are used. The nonlinear flow and stress sensitivity have an obvious influence on the interporosity flow. When the influence of nonlinear flow and stress sensitivity increases, the value of the shape factor and interporosity flow rate decrease. The shape factor becomes larger and the nonsteady state becomes longer after considering the influence of fracture pressure depletion. In addition, the interporosity rate will rise first to reach equilibrium and then decrease when the decline constant is very small. The new model can accurately characterize the interporosity flow in shale/tight reservoirs, which has important implications for well test interpretation, numerical simulation, and even optimization of the perforation cluster number.

AUTHOR INFORMATION

Corresponding Author

Shan Huang – Shale Gas Research Institute, Southwest Oil & Gas Field Company, PetroChina, Chengdu, Sichuan 610051, China; orcid.org/0000-0002-9886-6536; Email: cupbhs@163.com

Authors

Xinhua Ma – Research Institute of Petroleum Exploration & Development, PetroChina, Beijing 100083, China
Rui Yong – Southwest Oil & Gas Field Company, PetroChina, Chengdu, Sichuan 610051, China
Jianfa Wu – Shale Gas Research Institute, Southwest Oil & Gas Field Company, PetroChina, Chengdu, Sichuan 610051, China
Jian Zhang – Shale Gas Research Institute, Southwest Oil & Gas Field Company, PetroChina, Chengdu, Sichuan 610051, China
Tianpeng Wu – Shale Gas Research Institute, Southwest Oil & Gas Field Company, PetroChina, Chengdu, Sichuan 610051, China

Complete contact information is available at:

<https://pubs.acs.org/10.1021/acsomega.2c00027>

Notes

The authors declare no competing financial interest.

ACKNOWLEDGMENTS

The authors acknowledge the financial support by the Science and Technology Projects (kt2021-11-02-02) of PetroChina Exploration & Production Company.

REFERENCES

- (1) Zou, C.; Yang, Z.; Cui, J.; Zhu, R.; Hou, L.; Tao, S.; Yuan, X.; Wu, S.; Lin, S.; Wang, L.; Bai, B.; Yao, J. Formation mechanism, geological characteristics and development strategy of nonmarine shale oil in China. *Pet. Explor. Dev.* **2013**, *40*, 15–27.
- (2) Ji, J.; Yao, Y.; Huang, S.; Ma, X.; Zhang, S.; Zhang, F. Analytical model for production performance analysis of multi-fractured horizontal well in tight oil reservoirs. *J. Pet. Sci. Eng.* **2017**, *158*, 380–397.
- (3) He, Y.; Qin, J.; Cheng, S.; Chen, J. Estimation of fracture production and water breakthrough locations of multi-stage fractured horizontal wells combining pressure-transient analysis and electrical resistance tomography. *J. Pet. Sci. Eng.* **2020**, *194*, No. 107479.
- (4) He, Y. W.; Tang, Y.; Qin, J. Z.; Yu, W.; Wang, Y.; Sepehrnoori, K. Multi-Phase Rate Transient Analysis Considering Complex Fracture Networks. *SPE Annu. Tech. Conf. Exhib.* October 26–29, 2020.
- (5) Huang, S.; Li, W.; Wu, J.; Zhang, H.; Luo, Y. A study of the mechanism of nonuniform production rate in shale gas based on nonradioactive gas tracer technology. *Energy Sci. Eng.* **2020**, *8*, 2648–2658.
- (6) Barenblatt, G. I.; Zheltov, I. P.; Kochina, I. N. Basic concepts in the theory of seepage of homogeneous liquids in fissured rocks. *J. Appl. Math. Mech.* **1960**, *24*, 1286–1303.
- (7) Warren, J. E.; Root, P. J. The Behavior of naturally fractured reservoirs. *Soc. Pet. Eng. J.* **1963**, *3*, 245–255.
- (8) Kazemi, H.; Merrill, L. S., Jr.; Porterfield, K. L.; Zeman, P. R. Numerical simulation of water-oil flow in naturally fractured reservoirs. *SPE J.* **1976**, *16*, 317–326.
- (9) Thomas, L. K.; Dixon, T. N.; Pierson, R. G. Fractured reservoir simulation. *Soc. Pet. Eng. J.* **1983**, *23*, 42–54.
- (10) Ueda, Y.; Murata, S.; Watanabe, Y.; Funatsu, K. Investigation of the Shape Factor Used in the Dual-Porosity Reservoir Simulator. *SPE Asia-Pacific Conf.* 1989.
- (11) Coats, K. H. Implicit compositional simulation of single-porosity and dual-porosity reservoirs. *SPE Symposium on Reservoir Simulation.* 1989.
- (12) de Swaan. Influence of shape and skin of matrix-rock blocks on pressure transients in fractured reservoirs. *SPE Form. Eval.* **1990**, *5*, 344–352.
- (13) Kazemi, H.; Gilman, J. R. Multiphase flow in fractured petroleum reservoirs. *Flow Contam. Transp. Fract. Rock.* **1993**, *6*, 267–323.

- (14) Zimmerman, R. W.; Chen, G.; Hadgu, T.; Bodvarsson, G. S. A numerical dual-porosity model with semianalytical treatment of fracture/matrix flow. *Water Resour. Res.* **1993**, *29*, 2127–2137.
- (15) Quintard, M.; Whitaker, S. Transport in chemically and mechanically heterogeneous porous media. II: Comparison with numerical experiments for slightly compressible single-phase flow. *Adv. Water Resour.* **1996**, *19*, 49–60.
- (16) Bourbiaux, B.; Granet, S.; Landereau, P.; Noetinger, B.; Sarda, S.; Sabathier, J. C. Scaling up matrix-fracture transfers in dual-porosity models: theory and application. *SPE Technical Conference and Exhibition*. 1999, 15.
- (17) Noetinger, B.; Estebenet, T. Up-scaling of double porosity fractured media using continuous-time random walks methods. *Transp. Porous Media*. **2000**, *39*, 315–337.
- (18) Sarda, S.; Jeannin, L.; Basquet, R.; Bourbiaux, B. Hydraulic characterization of fractured reservoirs: simulation on discrete fracture models. *SPE Reservoir Eval. Eng.* **2002**, *5*, 154–162.
- (19) Rasmussen, M. L.; Civan, F. Full, short-, and long-time analytical solutions for hindered matrix-fracture transfer models of naturally fractured petroleum reservoirs. *SPE Production and Operations Symposium*. 2003.
- (20) Chang, M. M. *Deriving the shape factor of a fractured rock matrix*. National Inst. for Petroleum and Energy Research: Bartlesville, OK (United States). 1993.
- (21) Lim, K. T.; Aziz, K. Matrix-fracture transfer shape factors for dual-porosity simulators. *J. Pet. Sci. Eng.* **1995**, *13*, 169–178.
- (22) Rangel-German, E. R.; Kowsek, A. R. Time-dependent matrix-fracture shape factors for partially and completely immersed fractures. *J. Pet. Sci. Eng.* **2006**, *54*, 149–163.
- (23) Hassanzadeh, H.; Pooladi-Darvish, M. Effects of fracture boundary conditions on matrix-fracture transfer shape factor. *Transp. Porous Media*. **2006**, *64*, 51–71.
- (24) Ranjbar, E.; Hassanzadeh, H.; Chen, Z. Effect of fracture pressure depletion regimes on the dual-porosity shape factor for flow of compressible fluids in fractured porous media. *Adv. Water Resour.* **2011**, *34*, 1681–1693.
- (25) Ranjbar, E.; Hassanzadeh, H. Matrix–fracture transfer shape factor for modeling flow of a compressible fluid in dual-porosity media. *Adv. Water Resour.* **2011**, *34*, 627–639.
- (26) He, Y. M. *The shape factor study and application for fractured reservoir*; Chengdu University of Technology: Chengdu, 2007.
- (27) He, Y.; Chen, X.; Zhang, Y.; Yu, W. Modeling interporosity flow functions and shape factors in low-permeability naturally fractured reservoir. *J. Pet. Sci. Eng.* **2017**, *156*, 110–117.
- (28) Wang, L.; Yao, Y. D.; Huang, S.; Geng, D. D.; Liu, X. D.; Zhang, Y. Transient cross flow law for fractured tight oil reservoirs. *Fault Block Oil Gas Field* **2016**, *23*, 329–333.
- (29) Wang, L.; Yang, S.; Meng, Z.; Chen, Y.; Qian, K.; Han, W.; Wang, D. Time-dependent shape factors for fractured reservoir simulation: Effect of stress sensitivity in matrix system. *J. Pet. Sci. Eng.* **2018**, *163*, 556–569.
- (30) Liu, K.; Yin, D.; Sun, Y.; Xia, L. Analytical and experimental study of stress sensitivity effect on matrix / fracture transfer in fractured tight reservoir. *J. Pet. Sci. Eng.* **2020**, *195*, No. 107958.
- (31) Rostami, P.; Sharifi, M.; Dejam, M. Shape factor for regular and irregular matrix blocks in fractured porous media. *Pet. Sci.* **2020**, *17*, 136–152.
- (32) Abbasi, M.; Kazemi, A.; Sharifi, M. Modeling of transient shape factor in fractured reservoirs considering the effect of heterogeneity, pressure-dependent properties and quadratic pressure gradient. *Oil Gas Sci. Technol.* **2019**, *74*, 89–12.
- (33) Penuela, G.; Civan, F.; Hughes, R. G.; Wiggins, M. L. Time-dependent shape factors for interporosity flow in naturally fractured gas-condensate reservoirs. *SPE Gas Technology Symposium*. 2002.
- (34) Civan, F.; Rasmussen, M. L. Analytical hindered-matrix-fracture transfer models for naturally fractured petroleum reservoirs. *SPE International Petroleum Conference and Exhibition in Mexico*. 2002.
- (35) Golghanddashti, H. A new analytically derived shape factor for gas–oil gravity drainage mechanism. *J. Pet. Sci. Eng.* **2011**, *77*, 18–26.
- (36) Taabbodi, L.; Chen, Z. J.; Geiger, S. Transient shape factors for thermal flow simulation in naturally fractured reservoirs: a concept. *SPE Heavy and Extra Heavy Oil Conference: Latin America*. 2014.
- (37) Lei, H.; He, L.; Li, R.; Hu, Z.; He, J. Effects of boundary layer and stress sensitivity on the performance of low-velocity and one-phase flow in a shale oil reservoir: Experimental and numerical modeling approaches. *J. Pet. Sci. Eng.* **2019**, *180*, 186–196.
- (38) Huang, S.; Yao, Y.; Zhang, S.; Ji, J.; Ma, R. A fractal model for oil transport in tight porous media. *Transp. Porous Media*. **2018**, *121*, 725–739.
- (39) Huang, S.; Yao, Y. D.; Zhang, S.; Ji, J. H.; Wang, D. F. An effective permeability model for tight reservoirs. *The Chinese Congress of Theoretical and Applied Mechanics (CCTAM)*, 2017.
- (40) Wang, J.; Jia, A.; Wei, Y.; Qi, Y. Approximate semi-analytical modeling of transient behavior of horizontal well intercepted by multiple pressure-dependent conductivity fractures in pressure-sensitive reservoir. *J. Pet. Sci. Eng.* **2017**, *153*, 157–177.
- (41) Kong, X. Y. *Higher seepage mechanics*. 2nd edition; China University of Science and Technology Press: Hefei. 2010, 325–331.
- (42) Huang, S.; Yao, Y.; Zhang, S.; Ji, J.; Ma, R. Pressure transient analysis of multi-fractured horizontal wells in tight oil reservoirs with consideration of stress sensitivity. *Arab. J. Geosci.* **2018**, *11*, 285.
- (43) Huang, S.; Yao, Y.; Ma, R.; Wang, J. Analytical model for pressure and rate analysis of multi-fractured horizontal wells in tight gas reservoirs. *J. Pet. Explor. Prod. Technol.* **2019**, *9*, 383–396.
- (44) Clarkson, C. R.; Pedersen, P. K. Production analysis of Western Canadian unconventional light oil plays. *Canadian Unconventional Resources Conference*. 2011.